Nano Research
2022, 15(2): 959–964
ISSN 1998-0124 CN 11-5974/O4
https://doi.org/10.1007/s12274-021-3581-y

Research Article

Atomically dispersed N-coordinated Fe-Fe dual-sites with enhanced enzyme-like activities

Lei Jiao[1,§], Wei Ye[2,§], Yikun Kang[3,§], Yu Zhang[1], Weiqing Xu[1], Yu Wu[1], Wenling Gu[1], Weiyu Song[3] (✉), Yujie Xiong[4] (✉), and Chengzhou Zhu[1] (✉)

[1] *Key Laboratory of Pesticide and Chemical Biology of Ministry of Education, International Joint Research Center for Intelligent Biosensing Technology and Health, College of Chemistry, Central China Normal University, Wuhan 430079, China*
[2] *College of Material, Chemistry and Chemical Engineering, Hangzhou Normal University, Hangzhou 311121, China*
[3] *State Key Laboratory of Heavy Oil Processing, China University of Petroleum, Beijing 102249, China*
[4] *Hefei National Laboratory for Physical Sciences at the Microscale, Collaborative Innovation Center of Chemistry for Energy Materials (iChEM), School of Chemistry and Materials Science, and National Synchrotron Radiation Laboratory, University of Science and Technology of China, Hefei 230026, China*
[§] *Lei Jiao, Wei Ye, and Yikun Kang contributed equally to this work.*

Received: 11 March 2021 / **Revised:** 18 April 2021 / **Accepted:** 6 May 2021

ABSTRACT

Replacement of enzymes with nanomaterials such as atomically dispersed metal catalysts is one of the most crucial steps in addressing the challenges in biocatalysis. Despite the breakthroughs of single-atom catalysts in enzyme-mimicking, a fundamental investigation on the development of an instructional strategy is still required for mimicking biatomic/multiatomic active sites in natural enzymes and constructing synergistically enhanced metal atom active sites. Herein, Fe_2NC catalysts with atomically dispersed Fe-Fe dual-sites supported by the metal-organic frameworks-derived nitrogen-doped carbon are employed as biomimetic catalysts to perform proof-of-concept investigation. The effect of Fe atom number toward typical oxidase (cytochrome C oxidase, NADH oxidase, and ascorbic acid oxidase) and peroxidase (NADH peroxidase and ascorbic acid peroxidase) activities is systematically evaluated by experimental and theoretical investigations. A peroxo-like O_2 adsorption in Fe_2NC nanozymes could accelerate the O–O activation and thus achieve the enhanced enzyme-like activities. This work achieves the vivid simulation of the enzyme active sites and provides the theoretical basis for the design of high-performance nanozymes. As a concept application, a colorimetric biosensor for the detection of S^{2-} in tap water is established based on the inhibition of enzyme-like activity of Fe_2NC nanozymes.

KEYWORDS

nanozymes, atomically dispersed dual-metal sites, oxidase-like activities, single-atom catalysis, sensors

1 Introduction

Nanozymes, the nanomaterials with enzyme-like catalytic activity, have caused great attention in the field of biosensing, biomedicines, and environmental science due to their splendid advantages in easy preparation, low cost, high stability, and tunable catalytic performance [1–5]. Since the first attempt of magnetic Fe_3O_4 nanoparticles with intrinsic peroxidase-like activities has been developed [6], various nanomaterials, such as noble metal nanostructures, carbon nanomaterials, and transition metal-based nanomaterials, have been discovered to exhibit enzyme-like properties [7–12]. However, conventional nanozymes always possess diversified size and morphology, complex composition and structures, resulting in some inevitable difficulties in the precise recognition of active sites and further understanding of the catalytic mechanism at the atomic scale.

Recently, due to the unique geometric/electronic structure, high metal atomic utilization efficiency, and the strong interaction between metal and support, single-atom catalysts (SACs) exhibit exceptional catalytic activity [13–22]. Among them, SACs with well-defined atomically dispersed active sites can mimic the catalytic activities of some metalloproteases, such as peroxidases, catalases, and oxidases, and they are defined as single-atom nanozymes [23–28]. Specifically, it is established that FeNC single-atom nanozymes can mimic oxidase activities, and corresponding mechanism analysis found that the Fe-based single site in FeNC single-atom nanozymes tends to adsorb only one oxygen atom of O_2, resulting in superoxo-like O_2 adsorption (Fig. S1 in the Electronic Supplementary Material (ESM)) [25, 29, 30]. Although these FeNC single-atom nanozymes have heme-like active sites, their electronic structures and coordination environments are still quite different from those of natural enzymes. For example, cytochrome c oxidase (CcO) as a typical heme-copper oxidase is the terminal enzyme with heme-copper hetero-binuclear active center, which could catalyze O_2 to H_2O *in vivo* and thus realize the preparation of adenosine triphosphate in aerobic organisms (Fig. S2 in the ESM) [31]. In this reaction, the peroxo-like O_2 configuration is bonded to the binuclear active center. The synergistic effect between the heme site and Cu_B site could accelerate the O–O cleavage and

Address correspondence to Chengzhou Zhu, czzhu@mail.ccnu.edu.cn; Weiyu Song, songwy@cup.edu.cn; Yujie Xiong, yjxiong@ustc.edu.cn

achieve the $4e^-/4H^+$ reduction of O_2 (Fig. S3 in the ESM) [32, 33]. Also, polyphenol oxidases could catalyze the oxidation of monophenols in the presence of O_2 molecules, where the process of O–O cleavage in polyphenol oxidases occurs at the double copper sites, similar to CcO [34, 35]. Significantly, atomically dispersed dual-metal atoms have demonstrated superior catalytic activity toward O_2 reduction in comparison to SACs, where atomic pairs with favorable electronic and geometric structures metal dimers are beneficial for the adsorption/desorption of the reaction intermediate and the cleavage of the O–O bonds [36–40]. The binuclear biocatalysis involved in natural systems and the exceptional catalytic activity of dual-atom catalysts inspire us to further investigate the enzyme-like activities of dual-atom catalysts, achieving the ultimate goal of vivid mimicking of natural enzymes.

Herein, to vividly mimic the binuclear active sites of natural enzymes, we employed the Fe_2NC nanozymes with Fe-Fe dimer as a coordination center on zeolitic imidazolate framework (ZIF-8)-derived nitrogen-doped porous carbon (Fe_2NC) as dual-atom nanozymes (Fig. 1). Both experimental and theoretical investigations revealed that Fe_2NC nanozymes exhibit higher oxidase and peroxidase-like activities than Fe_1NC (single-atom Fe on nitrogen-doped porous carbon). Owing to the unique peroxo-like O_2 adsorption configuration, Fe_2NC nanozymes could lengthen the distance of O–O bonding, accelerating the O–O cleavage and thus achieving the improvement of enzyme-like activities, which provide guidance in the design of high-efficient nanozymes. Finally, a colorimetric biosensor was established for the detection of S^{2-} in tap water based on the inhibition of Fe–N active sites.

2 Results and discussion

To accurately design the Fe_2NC nanozymes, the $Fe_2(CO)_9$ compounds with well-defined Fe_2 dimers as active centers were *in situ* encapsulated in zeolitic imidazolate framework (ZIF-8) to form $Fe_2(CO)_9$@ZIF-8 complex. After that, the $Fe_2(CO)_9$@ZIF-8 complex was calcined at 800 °C under the argon atmosphere. Accordingly, ZIF-8 was carbonized to form porous nitrogen-doped carbon, and $Fe_2(CO)_9$ in the cage of ZIF-8 was transformed into Fe_2 dimers anchored by nitrogen on the porous carbon, resulting in the formation of Fe_2NC nanozymes with atomically dispersed Fe_2 dimers [41]. Similarly, the Fe_1NC was also prepared by using iron acetylacetonate as precursors. All these samples possess dodecahedron features and are similar to ZIF-8-derived porous carbon (Figs. 2(a) and 2(d), and Fig. S4 in the ESM). Furthermore, the Fe_2 dimers interspersed in the support are directly observed from the image of the aberration-corrected high-angle annular dark-field scanning transmission electron microscopy (AC-HADDF-STEM, Fig. 2(e)). Similarly, single-atom Fe could be observed in their supports (Fig. 2(b)). Previously, the local structural information of Fe_xNC has been systematically investigated by the X-ray absorption fine structure spectra and corresponding theoretical calculations [41]. Fe_1NC had the single site Fe with four coordinated nitrogen atoms as active sites. The coordination numbers Fe-Fe bonding in Fe_2NC are 1.2. The active sites of Fe_2NC are atomically dispersed Fe_2N_6 species, and each Fe atom is bonded with three nitrogen atoms and one Fe atom. The fine structure information of Fe_xNC is displayed in Figs. 2(c) and 2(f). Accordingly, these nanozymes with well-defined active sites are the ideal models to investigate their enzyme-like activities to fill the gap between the nanoparticles and SACs.

In nature, oxidase can accelerate the O–O cleavage and achieve the reduction of O_2. We comprehensively investigated the CcO, NADH oxidase (NOX), and ascorbic acid oxidase (AAOX) activities of Fe_xNC (x = 1, 2) nanozymes, respectively, to evaluate their O_2 activation ability through UV–vis spectroscopy. Natural CcO can catalyze O_2 to oxidize ferrous cytochrome C (Cyt c) to produce ferric Cyt c through a direct $4e^-$ electron transfer process, resulting in the blue-shift of the absorption peak at around 410 nm and the decline of signal intensity at around 550 nm [42]. As displayed in Fig. 3(a), the experimental results demonstrate that Fe_2NC nanozymes can oxidize ferric Cyt c while Fe_1NC nanozymes have almost no CcO activity, indicating that dual-site Fe atoms in Fe_2NC nanozymes can efficiently activate O_2 and accelerate the electron transfer. The NOX activities of Fe_xNC nanozymes were also investigated. In detail, NOX can oxidize NADH to NAD^+, resulting in the decline of a characteristic peak at around 340 nm. As shown in Fig 3(b), Fe_2NC nanozymes exhibit higher NOX-like activities than Fe_1NC nanozymes, consisting well with the CcO-like activity of Fe_xNC nanozymes. In nature, NOX can be divided into NOX (I) and NOX (II). NOX (I) can catalyze NADH to NAD^+ by O_2 to produce H_2O_2 while NOX (II) can catalyze NADH to NAD^+ by O_2 to produce H_2O through a direct $4e^-$ process [43, 44]. We further investigated the intermediate products in enzyme-like catalytic reactions of Fe_xNC nanozymes. As displayed in Fig. S5(a) in the ESM, the additional H_2O_2 is detected by using horseradish peroxidase (HRP) and tetramethylbenzidine (TMB) as probes [45]. The generation of H_2O_2 is not observed in NOX-like catalytic processes, demonstrating that Fe_xNC nanozymes can mimic the activity of NOX (II).

We next investigated the AAOX-like activities of Fe_xNC nanozymes. Ascorbic acid (AA) could be oxidized by AAOX to produce dehydroascorbic acid in the presence of O_2, leading to the decline of signal intensity at around 265 nm (Fig. 3(c),

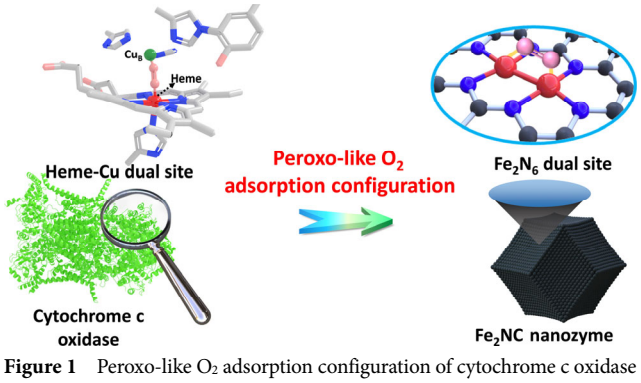

Figure 1 Peroxo-like O_2 adsorption configuration of cytochrome c oxidase and Fe_2NC nanozyme.

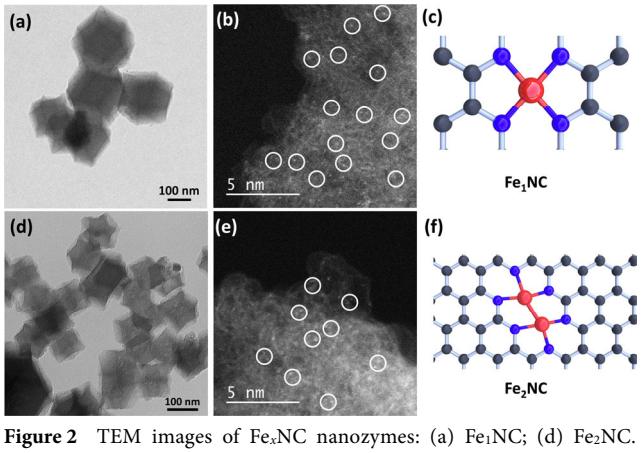

Figure 2 TEM images of Fe_xNC nanozymes: (a) Fe_1NC; (d) Fe_2NC. AC-HADDF-STEM images of Fe_xNC nanozymes: (b) Fe_1NC; (e) Fe_2NC. (c) and (f) active sites of Fe_xNC nanozymes.

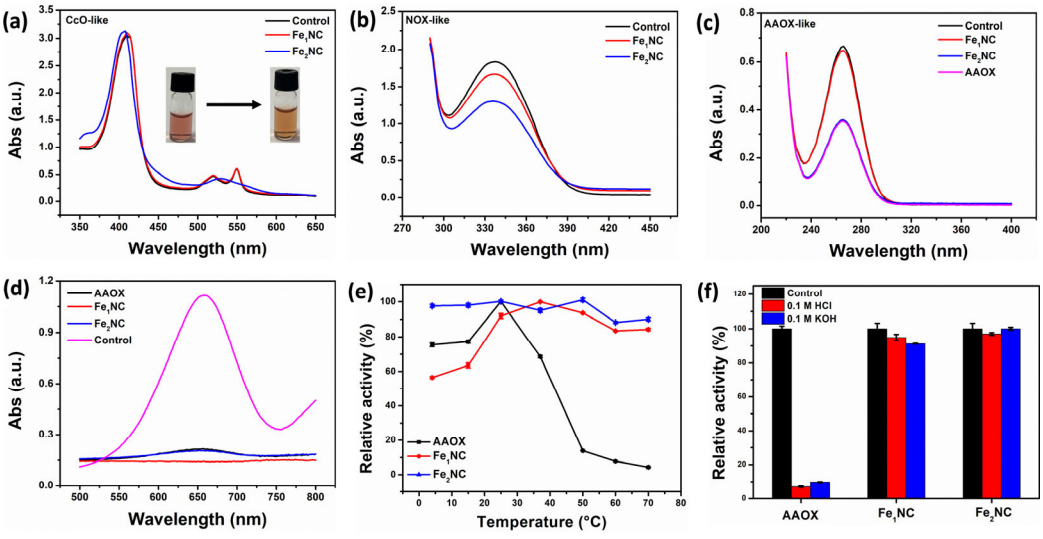

Figure 3 Oxidase activity comparison between Fe_1NC and Fe_2NC nanozymes. (a) UV–vis spectra of Cyt c solution in the presence of Fe_1NC and Fe_2NC nanozymes. (b) UV–vis spectra of NADH solution in the presence of Fe_1NC and Fe_2NC nanozymes. (c) UV–vis spectra of AA solution in the presence of Fe_1NC, Fe_2NC nanozymes and AAOX (test temperature = 25 °C). (d) UV–vis spectra of supernatant of AA-Fe_xNC nanozymes systems in HRP-TMB solution. Effects of temperature (e) and pH (f) for Fe_xNC nanozymes and AAOX.

pink line). It is found that Fe_2NC nanozymes possess higher AAOX-like activities than Fe_1NC nanozymes, further confirming that the O_2 molecules are more easily activated on dual-Fe sites in Fe_2NC nanozymes (Fig. 3(c)). As displayed in Fig. 3(d), the additional H_2O_2 is detected by using HRP and TMB as probes. Like natural AAOX, almost no H_2O_2 is detected in the enzyme-like reaction of Fe_xNC nanozymes, indicating that Fe_xNC nanozymes can direct catalyze AA and O_2 to produce dehydroascorbic acid and H_2O through a direct $4e^-$ path. To quantitatively evaluate the AAOX-like activities of Fe_xNC nanozymes, we established a calibration curve based on the enzyme activity of the natural AAOX (Fig. S5(b) in the ESM). Accordingly, the enzyme activity of Fe_2NC nanozymes is 18.9 U/mg, which is 23.33 times higher than that of Fe_1NC nanozymes (0.81 U/mg). Although the enzyme activity of Fe_2NC nanozymes still lags far behind that of natural AAOX (400 U/mg), Fe_xNC nanozymes exhibit higher tolerance at high temperatures and strong acid/basic conditions (Figs. 3(e) and 3(f)).

NADH peroxidases and AA peroxidases are the typical metalloproteases, which can accelerate the oxidation of NADH and AA in the presence of H_2O_2. As expected, Fe_2NC nanozymes possess higher NADH peroxidases-like and AA peroxidases-like activities than Fe_1NC nanozymes, indicating that H_2O_2 molecules are more easily activated on dual-Fe sites in Fe_2NC nanozymes (Figs. S6(a) and S6(b) in the ESM). Furthermore, the peroxidase-like activities of Fe_xNC nanozymes were quantitatively evaluated by the Michaelis-Menten kinetics in the colorimetric reactions. The V_{max} of Fe_2NC nanozymes (7.27×10^{-7} M/s) towards H_2O_2 is about 4.17 times higher than that of Fe_1NC nanozymes (Fig. S6(c) in the ESM). As for TMB, the V_{max} of Fe_2NC nanozymes (6.61×10^{-7} M/s) towards H_2O_2 is about 3.37 times higher than that of Fe_1NC nanozymes (Fig. S6(d) and Table S1 in the ESM). The excellent enzyme-like activities indicate that Fe_2NC nanozymes are more easily activate O_2 and H_2O_2 than Fe_1NC nanozymes, providing great opportunities to accurately tune metal active sites for boosting nanozyme activities.

The theoretical investigations were performed to reveal the catalytic nature of Fe_xNC nanozymes at the atomic scale. Previous work has confirmed that Fe_xNC nanozymes have comparable Fe loading (Fe_1NC: 0.35 wt.%; Fe_2NC: 0.38 wt.%) and specific surface area, demonstrating that the changes of enzyme-like activities are closely associated with the coordination environments of active sites [41]. As expected, the structural information of Fe_xNC nanozymes had been testified by the X-ray absorption fine structure spectra and corresponding theoretical calculations, which are beneficial for the establishment of theoretical models. There are two O_2 adsorption configurations including superoxo- and peroxo-like features are taken place on the surface of nanozymes. Previous works have proved that the O_2 adsorption configuration at the single Fe sites at Fe_1NC single-atom nanozymes is the superoxo-like structure [46]. Besides, some theoretical calculations have revealed that the peroxo-like O_2 adsorption configuration at the dual Fe sites can accelerate the O–O bonding cleavage, which could be attributed to the fact that more electrons are donated into the empty orbitals of O_2 toward better activation [41]. Based on the experimental results, almost no H_2O_2 was detected in the oxidase-like catalytic reactions. We concluded that the oxidation of Cyt c, NADH, and AA follows a four-electron transfer path. As shown in Fig. 4(a), we first established the O_2 molecule adsorption model toward Fe_xNC nanozymes. A superoxo-like adsorbed oxygen configuration was observed on Fe_1NC with an O–O bond length of 1.25 Å. As a comparison, O_2 on Fe_2NC tends to form a peroxo-like configuration with a larger O–O bond length of 1.45 Å, indicating that the peroxo-like configuration on Fe_2NC with the significantly extended distance of O–O bond can accelerate the O–O cleavage. To explore the origin of the enhanced enzyme-like activity, the differential charge density was performed to reveal the electronic structure of the active site. As can be seen in Fig. 4(b), the local electrons around the Fe_1NC and Fe_2NC active sites are all reduced, showing an oxidation state of Fe. The Bader charge of Fe (q_{Fe}) was calculated to reveal charge changes at the active site quantitatively. The Bader charge of Fe_1NC is 1.07, which is higher than that of Fe_2NC (q = 0.81). Obviously, the oxidation state of Fe decreases as the number of Fe atoms increases, where Fe_2NC shows the lowest oxidation state. Therefore, a lower oxidation state of Fe will result in a more effective activation of O_2. Furthermore, the project electronic density of states (PDOS) of oxygen adsorption state was calculated on the obtained Fe_xNC nanozymes (Fig. 4(c)). Meanwhile, the d-band centers of Fe and the p-band centers of O for each sample were also provided. The difference between the 3d band center of Fe and the 2p band center of O

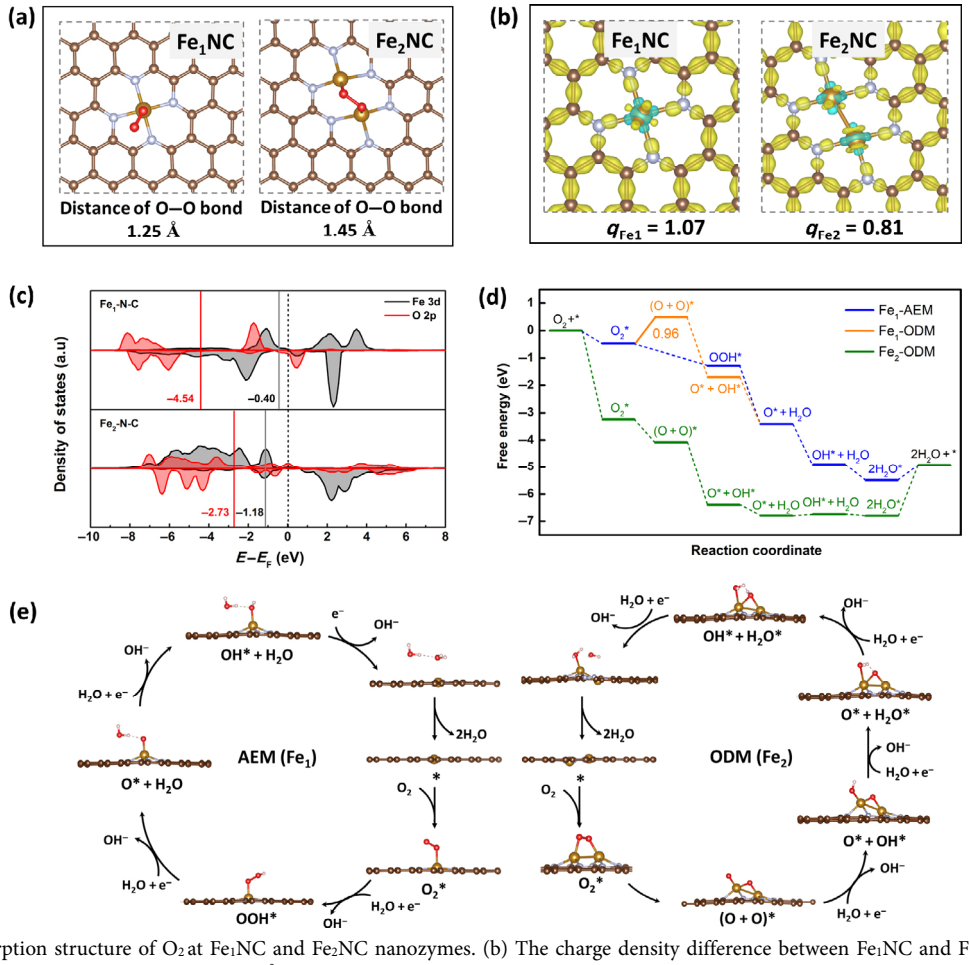

Figure 4 (a) Adsorption structure of O_2 at Fe_1NC and Fe_2NC nanozymes. (b) The charge density difference between Fe_1NC and Fe_2NC. Yellow (blue) isosurfaces denote an increase (decrease) of 0.02 e/Å^{-3} for electronic density. (c) The PDOS of oxygen adsorption state for Fe_1NC and Fe_2NC. The Fermi level is shown as the dash line. The d-band centers of Fe and the p-band centers of O are marked as solid lines for each sample. (d) Free energy diagram of oxygen reduction process on Fe_1NC and Fe_2NC via adsorption evolution mechanism (AEM) and oxygen dissociation mechanism (ODM). (e) The schematic diagram of oxygen reduction pathways following AEM (left) and ODM (right).

in Fe_2NC is smaller than that in Fe_1NC, indicating that the 3d orbital of Fe and the 2p orbital of O overlap widely at Fe_2NC active site, which is responsible for the strong adsorption of O_2.

The energy profile of oxygen reduction process is then calculated on Fe_1NC and Fe_2NC respectively (Fig. 4(d)). The oxygen reduction pathway was first simulated on the Fe_1NC sample via the adsorption evolution mechanism (AEM), where the intermediates evolved into OOH*, O*, and OH* in sequence after the adsorption of O_2 (left part of Fig. 4(e)). Notably, for the Fe_2NC site, adsorbed O_2 tends to dissociate directly rather than generate the OOH* species. Thereby, the oxygen reduction path on Fe_2 follows the proposed oxygen dissociation mechanism (ODM), where the intermediates evolved into O*, OH* and H_2O* in sequence after the adsorption of O_2 (right part of Fig. 4(e)). Obviously, the oxygen reduction intermediates can be more thermodynamically stable via ODM on the Fe_2 site, compared to that via AEM on Fe_1NC (Fig. 4(d)). Moreover, the oxygen reduction path via ODM was also calculated on the Fe_1NC site. The insurmountable O_2 dissociation energy (0.96 eV) indicates that the oxygen reduction path on the Fe_1NC site does not tend to follow the ODM. Therefore, due to the lower oxidation state of Fe_2NC site and the strong adsorption of O_2, the mechanism on Fe_2 is converted to ODM rather than AEM, which is more conducive to the oxygen reduction process and results in superior catalytic performance. Additionally, the process of H_2O_2 reduction was also investigated on Fe_1NC and Fe_2NC nanozymes (Figs. S7–S9 in the ESM). The calculated cracking energy of H_2O_2 on Fe_2NC (–5.48 eV) is larger than that on Fe_1NC (–2.01 eV), indicating the H_2O_2 can be effectively activated at the Fe_2NC active site.

Nanozymes as the efficient biosensing platforms have been widely investigated for the detection of small molecules (such as metal ions, glucose, and so on) [47, 48], cancer biomarkers [49], pathogens [50] and viruses [51], exhibiting satisfactory sensitivity and selectivity. In this work, as a concept application, we developed a colorimetric biosensor for the detection of S^{2-} in tap water based on the enzyme-like activities of Fe_2NC nanozymes. S^{2-} is the byproduct of petrochemical, leather, and food processing industries, being extensively released into the environment and thus resulting in environmental pollution [52, 53]. Also, the abnormal level of the S^{2-} derivative H_2S *in vivo* is closely associated with some diseases, such as Alzheimer's, Down's syndrome, and diabetes [54, 55]. Hence, sensitive and selective detection of S^{2-} plays a crucial role in the fields of environmental protection and human health. Herein, the proposed Fe_2NC nanozymes with enzyme-like activities were used to sensitively detect S^{2-} in tap water. The detection principle is displayed in Fig. 5(a). TMB as the chromophoric molecules could be oxidized by H_2O_2/O_2 with the help of Fe_2NC nanozymes as catalysts, generating a sharp blue peak at 652 nm. The S^{2-} could inhibit the enzyme-like activities of Fe_2NC nanozymes, causing the color decrease in absorbance. Some experimental conditions, such as nanozymes concentrations and incubation times, were optimized to amplify the sensitivity (Fig. S10 in the ESM). As expected, following the increment of S^{2-} concentrations from 1–800 μM, the absorbance values at

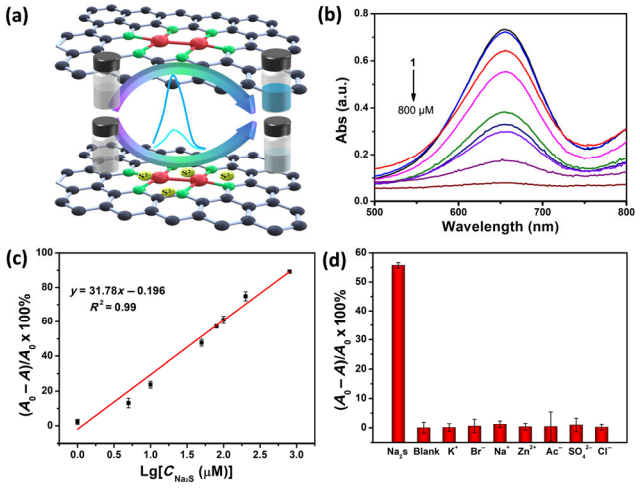

Figure 5 (a) Detection principle toward S^{2-} based on the enzyme-like activity of Fe_2NC nanozymes. (b) Absorbance spectra of the proposed colorimetric biosensor with different concentrations of S^{2-}. A calibration curve (c) and specificity (d) of the proposed colorimetric biosensor.

652 nm of oxTMB are gradually decreased (Fig. 5(b)). Accordingly, the calibration curve of color change ($A_0 - A/A_0$), responding to the logarithmic S^{2-} concentrations is established (Fig 5(c)). The limit of detection for S^{2-} is calculated as to be 0.61 μM. Also, the resultant colorimetric biosensor exhibits satisfactory selectivities in some anion and cation solutions (Fig. 5(d)). Furthermore, the standard addition recovery was used to evaluate the practical feasibility of this detection method. First, no S^{2-} is detected in the tap water. Then, the recoveries in Table S2 in the ESM are in the range of 94.21%–100.31%, demonstrating that this colorimetric biosensor has the potential for practical application.

3 Conclusions

To sum up, we found that Fe_2NC nanozymes with atomically dispersed Fe_2N_6 species as active sites could accelerate the O–O cleavage and thus achieve the enhanced oxidase-like and peroxidase-like activities. Theoretical investigations demonstrated that O_2 molecules are more likely to bind with Fe_2NC nanozymes through a peroxo-like O_2 adsorption configuration, which is similar to the natural heme-copper oxidase with the binuclear active sites. It is the first attempt that Fe_2NC dual-atom nanozymes exhibit higher enzyme-like activities than Fe_1NC single-atom nanozymes, which provides a theoretical basis for designing high-performance nanzymes. As a concept application, the Fe_2NC nanozymes were used to sensitively and selectively detect S^{2-} in tap water, exhibiting satisfactory feasibility in practical samples.

Acknowledgements

The authors gratefully acknowledge the financial support of National Natural Science Foundation of China (Nos. 22074049, 22004042, and 21503273), the Fundamental Research Funds for the Central Universities (Nos. CCNU20QN007 and CCNU20TS013) and the Program of Introducing Talents of Discipline to Universities of China (Nos. 111 program and B17019).

Electronic Supplementary Material: Supplementary material (experimental sections, TEM imaging, theoretical models, enzyme kinetics, and tables) is available in the online version of this article at https://doi.org/10.1007/s12274-021-3581-y.

References

[1] Wu, J. J. X.; Wang, X. Y.; Wang, Q.; Lou, Z. P.; Li, S. R.; Zhu, Y. Y.; Qin, L.; Wei, H. Nanomaterials with enzyme-like characteristics (nanozymes): Next-generation artificial enzymes (II). *Chem. Soc. Rev.* **2019**, *48*, 1004–1076.

[2] Huang, Y. Y.; Ren, J. S.; Qu, X. G. Nanozymes: Classification, catalytic mechanisms, activity regulation, and applications. *Chem. Rev.* **2019**, *119*, 4357–4412.

[3] Jiang, D. W.; Ni, D. L.; Rosenkrans, Z. T.; Huang, P.; Yan, X. Y.; Cai, W. B. Nanozyme: New horizons for responsive biomedical applications. *Chem. Soc. Rev.* **2019**, *48*, 3683–3704.

[4] Sun, H. J.; Zhou, Y.; Ren, J. S.; Qu, X. G. Carbon nanozymes: Enzymatic properties, catalytic mechanism, and applications. *Angew. Chem., Int. Ed.* **2018**, *57*, 9224–9237.

[5] Wang, Z. R.; Zhang, R. F.; Yan, X. Y.; Fan, K. L. Structure and activity of nanozymes: Inspirations for *de novo* design of nanozymes. *Mater. Today* **2020**, *41*, 81–119.

[6] Gao, L. Z.; Zhuang, J.; Nie, L.; Zhang, J. B.; Zhang, Y.; Gu, N.; Wang, T. H.; Feng, J.; Yang, D. L.; Perrett, S. et al. Intrinsic peroxidase-like activity of ferromagnetic nanoparticles. *Nat. Nanotechnol.* **2007**, *2*, 577–583.

[7] Xiang, H. J.; Feng, W.; Chen, Y. Single-atom catalysts in catalytic biomedicine. *Adv. Mater.* **2020**, *32*, 1905994.

[8] Fan, K. L.; Xi, J. Q.; Fan, L.; Wang, P. X.; Zhu, C. H.; Tang, Y.; Xu, X. D.; Liang, M. M.; Jiang, B.; Yan, X. Y. et al. *In vivo* guiding nitrogen-doped carbon nanozyme for tumor catalytic therapy. *Nat. Commun.* **2018**, *9*, 1440.

[9] Chong, Y.; Dai, X.; Fang, G.; Wu, R. F.; Zhao, L.; Ma, X. C.; Tian, X.; Lee, S.; Zhang, C.; Chen, C. Y. et al. Palladium concave nanocrystals with high-index facets accelerate ascorbate oxidation in cancer treatment. *Nat. Commun.* **2018**, *9*, 4861.

[10] Fang, G.; Li, W. F.; Shen, X. M.; Perez-Aguilar, J. M.; Chong, Y.; Gao, X. F.; Chai, Z. F.; Chen, C. Y.; Ge, C. C.; Zhou, R. H. Differential Pd-nanocrystal facets demonstrate distinct antibacterial activity against gram-positive and gram-negative bacteria. *Nat. Commun.* **2018**, *9*, 129.

[11] Xu, W. Q.; Kang, Y. K.; Jiao, L.; Wu, Y.; Yan, H. Y.; Li, J. L.; Gu, W. L.; Song, W. Y.; Zhu, C. Z. Tuning atomically dispersed Fe sites in metal-organic frameworks boosts peroxidase-like activity for sensitive biosensing. *Nano-Micro Lett.* **2020**, *12*, 184.

[12] Xi, J. Q.; Zhang, R. F.; Wang, L. M.; Xu, W.; Liang, Q.; Li, J. Y.; Jiang, J.; Yang, Y. L.; Yan, X. Y.; Fan, K. L. et al. A nanozyme-based artificial peroxisome ameliorates hyperuricemia and ischemic stroke. *Adv. Funct. Mater.* **2021**, *31*, 2007130.

[13] Wu, Y.; Wu, J. B.; Jiao, L.; Xu, W. Q.; Wang, H. J.; Wei, X. Q.; Gu, W. L.; Ren, G. X.; Zhang, N.; Zhang, Q. H. et al. Cascade reaction system integrating single-atom nanozymes with abundant Cu sites for enhanced biosensing. *Anal. Chem.* **2020**, *92*, 3373–3379.

[14] Xu, B. L.; Wang, H.; Wang, W. W.; Gao, L. Z.; Li, S. S.; Pan, X. T.; Wang, H. Y.; Yang, H. L.; Meng, X. Q.; Wu, Q. W. et al. A single-atom nanozyme for wound disinfection applications. *Angew. Chem., Int. Ed.* **2019**, *58*, 4911–4916.

[15] Cheng, N.; Li, J. C.; Liu, D.; Lin, Y. H.; Du, D. Single-atom nanozyme based on nanoengineered Fe–N–C catalyst with superior peroxidase-like activity for ultrasensitive bioassays. *Small* **2019**, *15*, 1901485.

[16] Zhu, C. Z.; Fu, S. F.; Shi, Q. R.; Du, D.; Lin, Y. H. Single-atom electrocatalysts. *Angew. Chem., Int. Ed.* **2017**, *56*, 13944–13960.

[17] Chen, M.; Zhou, H.; Liu, X. K.; Yuan, T. W.; Wang, W. Y.; Zhao, C.; Zhao, Y. F.; Zhou, F. Y.; Wang, X.; Xue, Z. G. et al. Single iron site nanozyme for ultrasensitive glucose detection. *Small* **2020**, *16*, 2002343.

[18] Zhao, C.; Xiong, C.; Liu, X. K.; Qiao, M.; Li, Z. J.; Yuan, T. W.; Wang, J.; Qu, Y. T.; Wang, X. Q.; Zhou, F. Y. et al. Unraveling the enzyme-like activity of heterogeneous single atom catalyst. *Chem. Commun.* **2019**, *55*, 2285–2288.

[19] Luo, X.; Wei, X. Q.; Wang, H. J.; Gu, W. L.; Kaneko, T.; Yoshida, Y.; Zhao, X.; Zhu, C. Z. Secondary-atom-doping enables robust Fe–N–C single-atom catalysts with enhanced oxygen reduction reaction. *Nano-Micro Lett.* **2020**, *12*, 163.

[20] Gao, C.; Low, J. X.; Long, R.; Kong, T. T.; Zhu, J. F.; Xiong, Y. J.

Heterogeneous single-atom photocatalysts: Fundamentals and applications. *Chem. Rev.* **2020**, *120*, 12175–12216.
[21] Zhang, L. W.; Long, R.; Zhang, Y. M.; Duan, D. L.; Xiong, Y. J.; Zhang, Y. J.; Bi, Y. P. Direct observation of dynamic bond evolution in single-atom Pt/C_3N_4 catalysts. *Angew. Chem., Int. Ed.* **2020**, *59*, 6224–6229.
[22] Shen, L. H.; Ye, D. X.; Zhao, H. B.; Zhang, J. J. Perspectives for single-atom nanozymes: Advanced synthesis, functional mechanisms, and biomedical applications. *Anal. Chem.* **2021**, *93*, 1221–1231.
[23] Jiao, L.; Wu, J. B.; Zhong, H.; Zhang, Y.; Xu, W. Q.; Wu, Y.; Chen, Y. F.; Yan, H. Y.; Zhang, Q. H.; Gu, W. L. et al. Densely isolated FeN_4 sites for peroxidase mimicking. *ACS Catal.* **2020**, *10*, 6422–6429.
[24] Jiao, L.; Yan, H. Y.; Wu, Y.; Gu, W. L.; Zhu, C. Z.; Du, D.; Lin, Y. H. When nanozymes meet single-atom catalysis. *Angew. Chem., Int. Ed.* **2020**, *59*, 2565–2576.
[25] Huang, L.; Chen, J. X.; Gan, L. F.; Wang, J.; Dong, S. J. Single-atom nanozymes. *Sci. Adv.* **2019**, *5*, eaav5490.
[26] Jiao, L.; Xu, W. Q.; Yan, H. Y.; Wu, Y.; Liu, C. R.; Du, D.; Lin, Y. H.; Zhu, C. Z. Fe–N–C single-atom nanozymes for the intracellular hydrogen peroxide detection. *Anal. Chem.* **2019**, *91*, 11994–11999.
[27] Jiao, L.; Xu, W. Q.; Zhang, Y.; Wu, Y.; Gu, W. L.; Ge, X. X.; Chen, B. B.; Zhu, C. Z.; Guo, S. J. Boron-doped Fe–N–C single-atom nanozymes specifically boost peroxidase-like activity. *Nano Today* **2020**, *35*, 100971.
[28] Zhang, X. L.; Li, G. L.; Chen, G.; Wu, D.; Zhou, X. X.; Wu, Y. N. Single-atom nanozymes: A rising star for biosensing and biomedicine. *Coord. Chem. Rev.* **2020**, *418*, 213376.
[29] Wu, Y.; Jiao, L.; Luo, X.; Xu, W. Q.; Wei, X. Q.; Wang, H. J.; Yan, H. Y.; Gu, W. L.; Xu, B. Z.; Du, D. et al. Oxidase-like Fe–N–C single-atom nanozymes for the detection of acetylcholinesterase activity. *Small* **2019**, *15*, 1903108.
[30] Wang, Y.; Zhang, Z. W.; Jia, G. R.; Zheng, L. R.; Zhao, J. X.; Cui, X. Q. Elucidating the mechanism of the structure-dependent enzymatic activity of Fe–N/C oxidase mimics. *Chem. Commun.* **2019**, *55*, 5271–5274.
[31] Adam, S. M.; Wijeratne, G. B.; Rogler, P. J.; Diaz, D. E.; Quist, D. A.; Liu, J. J.; Karlin, K. D. Synthetic Fe/Cu complexes: Toward understanding heme-copper oxidase structure and function. *Chem. Rev.* **2018**, *118*, 10840–11022.
[32] Schaefer, A. W.; Roveda, A. C. Jr.; Jose, A.; Solomon, E. I. Geometric and electronic structure contributions to O–O cleavage and the resultant intermediate generated in heme-copper oxidases. *J. Am. Chem. Soc.* **2019**, *141*, 10068–10081.
[33] Schaefer, A. W.; Kieber-Emmons, M. T.; Adam, S. M.; Karlin, K. D.; Solomon, E. I. Phenol-induced O–O bond cleavage in a low-spin heme–peroxo–copper complex: Implications for O_2 reduction in heme–copper oxidases. *J. Am. Chem. Soc.* **2017**, *139*, 7958–7973.
[34] Li, M. H.; Chen, J. X.; Wu, W. W.; Fang, Y. X.; Dong, S. J. Oxidase-like MOF-818 nanozyme with high specificity for catalysis of catechol oxidation. *J. Am. Chem. Soc.* **2020**, *142*, 15569–15574.
[35] Mishra, B. B.; Gautam, S. Polyphenol oxidases: Biochemical and molecular characterization, distribution, role and its control. *Enzyme Eng.* **2016**, *5*, 1000141.
[36] Wang, J.; You, R.; Zhao, C.; Zhang, W.; Liu, W.; Fu, X. P.; Li, Y. Y.; Zhou, F. Y.; Zheng, X. S.; Xu, Q. et al. N-coordinated dual-metal single-site catalyst for low-temperature CO oxidation. *ACS Catal.* **2020**, *10*, 2754–2761.
[37] Wang, J.; Huang, Z. Q.; Liu, W.; Chang, C. R.; Tang, H. L.; Li, Z. J.; Chen, W. X.; Jia, C. J.; Yao, T.; Wei, S. Q. et al. Design of N-coordinated dual-metal sites: A stable and active Pt-free catalyst for acidic oxygen reduction reaction. *J. Am. Chem. Soc.* **2017**, *139*, 17281–17284.
[38] Tian, S. B.; Fu, Q.; Chen, W. X.; Feng, Q. C.; Chen, Z.; Zhang, J.; Cheong, W. C.; Yu, R.; Gu, L.; Dong, J. C. et al. Carbon nitride supported Fe_2 cluster catalysts with superior performance for alkene epoxidation. *Nat. Commun.* **2018**, *9*, 2353.
[39] Xiao, M. L.; Zhang, H.; Chen, Y. T.; Zhu, J. B.; Gao, L. Q.; Jin, Z.; Ge, J. J.; Jiang, Z.; Chen, S. L.; Liu, C. P. et al. Identification of binuclear Co_2N_5 active sites for oxygen reduction reaction with more than one magnitude higher activity than single atom CoN_4 site. *Nano Energy* **2018**, *46*, 396–403.
[40] Lu, Z. Y.; Wang, B.; Hu, Y. F.; Liu, W.; Zhao, Y. F.; Yang, R. O.; Li, Z. P.; Luo, J.; Chi, B.; Jiang, Z. et al. An isolated zinc–cobalt atomic pair for highly active and durable oxygen reduction. *Angew. Chem., Int. Ed.* **2019**, *58*, 2622–2626.
[41] Ye, W.; Chen, S. M.; Lin, Y.; Yang, L.; Chen, S. J.; Zheng, X. S.; Qi, Z. M.; Wang, C. M.; Long, R.; Chen, M. et al. Precisely tuning the number of Fe atoms in clusters on N-doped carbon toward acidic oxygen reduction reaction. *Chem* **2019**, *5*, 2865–2878.
[42] Singh, N.; Mugesh, G. $CeVO_4$ nanozymes catalyze the reduction of dioxygen to water without releasing partially reduced oxygen species. *Angew. Chem., Int. Ed.* **2019**, *58*, 7797–7801.
[43] Kang, T. S.; Korber, D. R.; Tanaka, T. Influence of oxygen on NADH recycling and oxidative stress resistance systems in *Lactobacillus* panis PM1. *AMB Express* **2013**, *3*, 10.
[44] Jia, B. L.; Park, S. C.; Lee, S.; Pham, B. P.; Yu, R.; Le, T. L.; Han, S. W.; Yang, J. K.; Choi, M. S.; Baumeister, W. et al. Hexameric ring structure of a thermophilic archaeon NADH oxidase that produces predominantly H_2O. *FEBS J.* **2008**, *275*, 5355–5366.
[45] Jiao, L.; Xu, W. Q.; Yan, H. Y.; Wu, Y.; Gu, W. L.; Li, H.; Du, D.; Lin, Y. H.; Zhu, C. Z. A dopamine-induced Au hydrogel nanozyme for enhanced biomimetic catalysis. *Chem. Commun.* **2019**, *55*, 9865–9868.
[46] Zhang, J. Q.; Zhao, Y. F.; Chen, C.; Huang, Y. C.; Dong, C. L.; Chen, C. J.; Liu, R. S.; Wang, C. Y.; Yan, K.; Li, Y. D. et al. Tuning the coordination environment in single-atom catalysts to achieve highly efficient oxygen reduction reactions. *J. Am. Chem. Soc.* **2019**, *141*, 20118–20126.
[47] Karim, M. N.; Anderson, S. R.; Singh, S.; Ramanathan, R.; Bansal, V. Nanostructured silver fabric as a free-standing *Nanozyme* for colorimetric detection of glucose in urine. *Biosens. Bioelectron.* **2018**, *110*, 8–15.
[48] Liu, Y.; Ding, D.; Zhen, Y. L.; Guo, R. Amino acid-mediated "turn-off/turn-on" nanozyme activity of gold nanoclusters for sensitive and selective detection of copper ions and histidine. *Biosens. Bioelectron.* **2017**, *92*, 140–146.
[49] Xi, Z.; Cheng, X.; Gao, Z. Q.; Wang, M. J.; Cai, T.; Muzzio, M.; Davidson, E.; Chen, O.; Jung, Y.; Sun, S. H. et al. Strain effect in palladium nanostructures as nanozymes. *Nano Lett.* **2020**, *20*, 272–277.
[50] Weerathunge, P.; Ramanathan, R.; Torok, V. A.; Hodgson, K.; Xu, Y.; Goodacre, R.; Behera, B. K.; Bansal, V. Ultrasensitive colorimetric detection of murine norovirus using *Nanozyme* aptasensor. *Anal. Chem.* **2019**, *91*, 3270–3276.
[51] Oh, S.; Kim, J.; Tran, V. T.; Lee, D. K.; Ahmed, S. R.; Hong, J. C.; Lee, J.; Park, E. Y.; Lee, J. Magnetic nanozyme-linked immunosorbent assay for ultrasensitive influenza a virus detection. *ACS Appl. Mater. Interfaces* **2018**, *10*, 12534–12543.
[52] Li, Y. H.; Fang, Y. S.; Gao, W. Q.; Guo, X. J.; Zhang, X. M. Porphyrin-based porous organic polymer as peroxidase mimics for sulfide-ion colorimetric sensing. *ACS Sustainable Chem. Eng.* **2020**, *8*, 10870–10880.
[53] Singh, S.; Mitra, K.; Shukla, A.; Singh, R.; Gundampati, R. K.; Misra, N.; Maiti, P.; Ray, B. Brominated graphene as mimetic peroxidase for sulfide ion recognition. *Anal. Chem.* **2017**, *89*, 783–791.
[54] Suzuki, K.; Olah, G.; Modis, K.; Coletta, C.; Kulp, G.; Gerö, D.; Szoleczky, P.; Chang, T. J.; Zhou, Z. M.; Wu, L. Y. et al. Hydrogen sulfide replacement therapy protects the vascular endothelium in hyperglycemia by preserving mitochondrial function. *Proc. Natl. Aca. Sci. USA* **2011**, *108*, 13829–13834.
[55] McGeer, E. G.; McGeer, P. L. Neuroinflammation in Alzheimer's disease and mild cognitive impairment: A field in its infancy. *J. Alzheimer's Dis.* **2010**, *19*, 355–361.